Volume 1 | Number 1 | Jan 2013 | Pages 1–100

CrystEngComm

www.rsc.org/crystengcomm

ROYAL SOCIETY OF CHEMISTRY

ROYAL SOCIETY OF CHEMISTRY

www.rsc.org/crystengcomm

Microstructures and Cl2-sensing performances of Zn-doped In2O3 hollow spheres
25x11mm (600 x 600 DPI)

PAPER

Zn-doped In$_2$O$_3$ hollow spheres: mild solution reaction synthesis and enhanced Cl$_2$ sensing performance

Pei Li, Huiqing Fan*, Yu Cai, Mengmeng Xu

Zn-doped In$_2$O$_3$ hollow spheres have been prepared by a facile chemical route under an even low temperature of 80 °C without any surfactant and template. Its morphological feature was characterized as self-assembled hollow spheres with a diameter of 200-300 nm, and it was observed that the amount of Zn-doped significantly affects the overall morphology. Furthermore, the analysis of N$_2$ adsorption/desorption tests showed that the Zn-doped In$_2$O$_3$ hollow spheres (the molar ratio of In/Zn is 9:1) adsorbed the largest amount of N$_2$ and had the biggest specific surface area (26.4 m^2/g), which contributed to the improvement of the gas sensing characteristics. Finally, gas sensing characteristics of the obtained products were studied. The results demonstrated that the sensors based on Zn-doped In$_2$O$_3$ structures exhibited a higher response to Cl$_2$ than those without Zn and the In/Zn = 9:1 (molar ratio) sample showed the highest response. The sensor based on Zn-doped In$_2$O$_3$ hollow spheres (the molar ratio of In/Zn is 9:1) exhibited the highest response of 94.7 ± 8.6 for 5 ppm Cl$_2$. The high response, quick response-recovery behaviour and excellent stability imply good potential for practical applications. The formation mechanism and gas sensing mechanism were studied.

Introduction

Gas sensors have been used for industrial process controls, for the detection of toxic environmental pollutants, in human health, and for the prevention of hazardous gas leaks, which comes from the manufacturing processes [1-4]. Indium oxide (In$_2$O$_3$), as an n-type semiconductor with a direct band gap of 3.55-3.75 eV [5], has been used extensively for gas sensing of NH$_3$ [6], H$_2$ [7], CO [8, 9], C$_2$H$_5$OH [10, 11], O$_3$ [12], etc. Cl$_2$ is one of air pollutant and the detection of dilute Cl$_2$ gas in exhaust would prevent the production of toxic compounds such as dioxin. However, the Cl$_2$ gas sensing properties of In$_2$O$_3$ have rarely been investigated so far.

Up to now, various morphologies of In$_2$O$_3$ have been fabricated, including nanofibers [13], nanotubes [14, 15], nanosheets [16], nanorods [17, 18], nanoflowers [19, 20], nanotowers [21], and so on. In addition to the current investigations on the above nanomaterials, hollow spheres, as typical three-dimensional curved structures with inner cavities, are of much importance because of their unique properties of low density, high specific surface area, and good permeation, and their potential applications in various areas [22, 23]. So far, hollow spheres of many materials have been fabricated through various methods, including template assisted synthesis, direct evacuations with Ostwald ripening, and the Kirkendall effect. Template-assisted synthesis is usually adopted for the preparation of hollow spheres [24]. However, the high cost, low yield, and complexity that accompany the introduction of templates have limited the practical application of these approaches. Therefore, it is still a major challenge to develop a facile and template-free route for the mass preparation of inorganic hollow structures.

Herein, we report a facile chemical route for the preparation of Zn-doped In$_2$O$_3$ hollow spheres with an appropriate Zn-doped amount. The obtained materials were characterized by the X-ray powder diffraction (XRD), the scanning electron microscopy (SEM), the transmission electron microscopy (TEM), the inductively coupled plasma mass spectrometry (ICP-MS), and the N$_2$ adsorption/desorption. The gas sensing properties of the resulting materials have also been investigated in detail. The introduction of a small quantity of Zn in the reaction system was found to play an important role in the particle size and morphology of Zn-doped In$_2$O$_3$ hollow spheres, consequently, which improved the sensing properties of the Cl$_2$ dramatically.

Experimental

Materials

The chemical reagents indium nitrate hydrate (In(NO$_3$)$_3$·4.5H$_2$O), zinc nitrate hydrate (Zn(NO$_3$)$_2$·6H$_2$O), anhydrous ethanol (C$_2$H$_5$OH), formamide, ammonium hydroxide (NH$_3$·H$_2$O) were of analytical grade and used without further purification (Sinopharm Chemical Reagent Co., Ltd, Shanghai, China).

Synthesis

Zn-doped In$_2$O$_3$ hollow spheres were synthesized by situ growth method. In a typical synthesis process, 1.5 mmol of In(NO$_3$)$_3$·4.5H$_2$O was dissolved in 46 ml anhydrous ethanol and a transparent solution I was obtained. Afterwards, 4 ml formamide was added dropwise into the solution I under vigorous stirring to

produce solution II. Then the solution II was transferred into a fixed three-neck flask. 2 ml $Zn(NO_3)_2$ hydrous solution with different concentration was added dropwise into the solution II under magnetic stirring. Then, ammonium hydroxide (1 mol/L) was slowly dripped into the solution II under stirring until the pH reaches 9. The resulting mixture was kept at 80 °C for 2 h. The white precipitates were separated by centrifugation, washed with distilled water and anhydrous ethanol for several times, and dried at 80 °C for 4 h. Finally, Zn-doped In_2O_3 hollow spheres were obtained after calcination at 500 °C for 2 h. We refer to these samples as S1, S2, S3, S4, S5 and S6, representing pure In_2O_3, and the In/Zn molar ratios of 15:1, 12:1, 9:1, 7:1 and 5:1, respectively.

Characterization

The phase structure and purity of the as-synthesized materials were examined by X-ray diffraction (XRD; X'pert PRO MPD, Philips, Eindhoven, The Netherlands) with Cu-Kα radiation (λ = 1.5406 Å) at 40 kV, 30 mA over the 2θ range 10-70°. The morphology of the obtained samples were investigated by using field emission scanning electron microscopy (FE-SEM; JSM-6701F, JEOL, Tokyo, Japan), and high resolution transmission electron microscopy (HRTEM; Tecnai F30G2, FEI, Hillsboro, OR, USA) operated at 300 kV accelerating voltage. Energy-dispersive X-ray (EDX) spectroscopy was also performed by using a microanalysis detector (X-MaxN 80 T, Oxford Instrument, Oxfordshire, UK). An inductively coupled plasma mass spectrometry (ICP-MS; 7500A, Agilent, Santa Clara, CA, USA) was used for simultaneous multi-element detection of Zn. The analytical parameters of the ICP-MS instrument are summarized in Table 1. The specific surface area of the In_2O_3 structures was obtained by full analysis of N_2 adsorption/desorption tests (V-Sorb 2800P, Gold APP Instruments Corporation, Beijing, China).

Table 1 Analytical parameters of the ICP-MS instrument

Nebulizer	Babington type
Spray chamber	Quarts, double pass
RF generator	Frequency: 10 MHz, power output: 1220 W
Air flow rate (L/min)	20
Auxiliary gas flow rate (L/min)	0.9
Nebuliser gas flow rate (L/min)	1-1.2
Sample uptake rate (μL/min)	400
Number of replicates	3
Integration time (s)	0.1
Wavelengths (nm)	206.200

Gas sensor fabrication and measurements

The basic fabricated process is as follows [25]. The as-obtained Zn-doped In_2O_3 hollow structures were slightly grinded with α-terpineol in an agate mortar to form a gas sensing paste. The paste used as sensitive body was coated on an alumina tube with Au electrodes and platinum wires, then dried under IR light for several minutes in air, and then sintered at 500 °C for 2 h. A Ni-Cr alloy crossing alumina tube was used as a heating resistor which ensured both substrate heating and temperature controlling. In order to improve their stability, the gas sensors were aged at 300 °C for 240 h in air.

The gas sensing properties were tested by using a gas response instrument (HW-30A, Hanwei Ltd, Zhengzhou, China). The gas sensing properties of Zn-doped In_2O_3 hollow structures tested in the glass test chamber, and the volume of test chamber is 15 L. In the measuring electric circuit of gas sensor, a load resistor is connected in series with a gas sensor. The circuit voltage V_c is 5 V, and the output voltage (V_{out}) is the terminal voltage of the load resistor R_L. The working temperature of sensor is adjusted by varying the heating voltage V_h. When a given amount of tested gas was injected into a chamber, the resistance of sensor changed. As a result, the output voltage changed. Gas response (S) is defined as follows: Response = R_g / R_a. where the R_g and R_a are the resistance values measured in oxidizing atmosphere and air, respectively. For each sample, three sensors were made by the same fabrication process, each sensor was tested three times in the gas sensing testing process, and the gas response values were the average value.

Results and discussion

Crystalline structure and morphology

Fig. 1 shows the X-ray diffraction patterns of pure In_2O_3 and Zn-doped In_2O_3 hollow structures with different molar ratios of In/Zn. All the strong and sharp diffraction peaks can be readily indexed to a cubic lattice [space group la-3(206)] of pure In_2O_3 according to the Joint Committee on Powder Diffraction Standards (JCPDS) data card No. 06-0416. No other phases such as ZnO, $In(NO_3)_3 \cdot 4.5H_2O$, or InOOH were detected, and the powder is pure In_2O_3 phase product. The cell parameters and the size of the crystallites determined with the Scherrer formula were listed in Table 2. As can be seen, the above calculated lattice constants are well compatible with the literature values of a=b=c=10.118 Å (bcc-In_2O_3, JCPDS 06-0416). Scherrer formula for finding the crystallite size (D) is given as: D = $(K\lambda) / (\beta cos\theta)$. Where, K is the Scherrers constant and has the value 0.89, λ is the wavelength of the radiation (1.5418 Å), β is the forward width at half maximum (FWHM) (radian) and θ is the half value of the Bragg diffraction angle in the XRD pattern (degree).
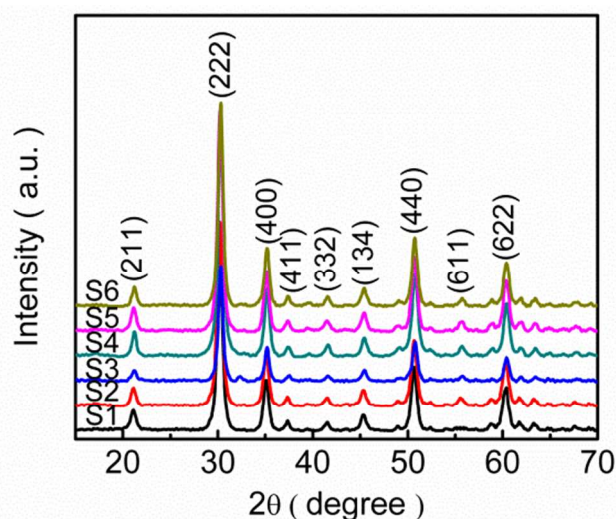
Fig.1 XRD patterns of pure In_2O_3 and Zn-doped In_2O_3 structures

The actual molar ratio of In/Zn in Zn-doped In_2O_3 structures was determined by using ICP-MS instrument, as is shown in Table 2. The results show that the real Zn ratio is lower than the theoretical ratio, and is lower than 1.

Table 2 Cell parameters and the size of pure In_2O_3 and Zn-doped In_2O_3 structures, and the actual Zn contents

Sample	In_2O_3(cell parameters)	D	theoretical In/Zn	actual In/Zn
	a = b= c (Å)	(nm)	(molar ratio)	(molar ratio)
S1	10.1181	6.83	–	–
S2	10.1182	6.90	15:1	15:0.61
S3	10.1193	6.67	12:1	12:0.66
S4	10.1184	6.54	9:1	9:0.72
S5	10.1176	7.28	7:1	7:0.75
S6	10.1187	7.72	5:1	5:0.57
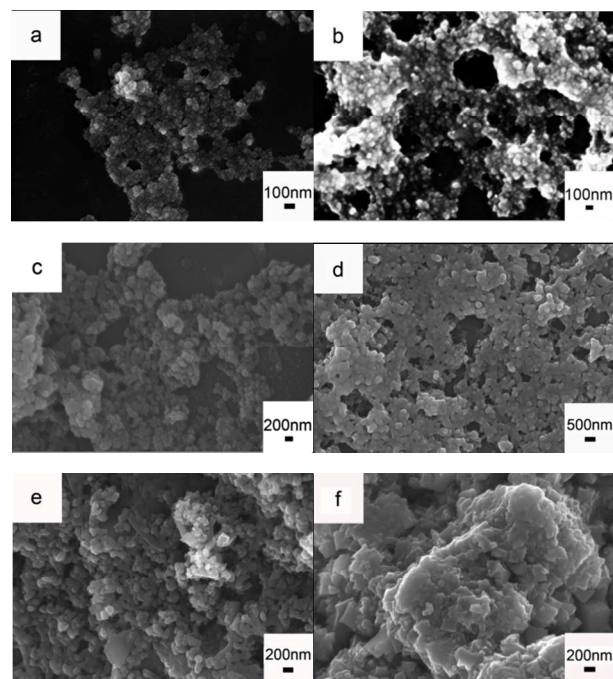
Fig.2 SEM images of (a) S1, (b) S2, (c) S3, (d) S4, (e) S5 and (f) S6

Fig. 2(a-f) shows the SEM images of pure In_2O_3 and Zn-doped In_2O_3 hollow structures with different In/Zn molar ratios. It indicated that the obtained materials are formed by many spheres and Zn plays an important role in controlling the particle size and morphology. As depicted in Fig. 2a, pure In_2O_3 consists of large regular aggregates of nanospheres with a diameter of 50-100 nm. Upon the introduction of Zn, the diameter of In_2O_3 spheres enlarged, which is in contrast to the sample without Zn (Fig. 2a), as shown in the Fig. 2(b-f). When the In/Zn molar ratio is 9:1, the diameter is 200-300 nm (Fig. 2d). With further increasing of Zn-doped amount, the diameter of spheres enlarged further, and aggregated to form some irregular spheres and cubes, as can be seen from Fig. 2(e-f). When the In/Zn molar ratio was 5:1, the diameter is 200-600 nm (Fig. 2f), the larger diameter and irregular shape may destroy the morphology and affect the Cl_2 sensing performance.

Compare the SEM images before and after calcination, the hollow spheres remained the similar spherical shape and diameter, indicate that calcination never destroy the surface topography, as shown in Fig 3a and Fig 3d. To give further insight into the morphology and structure of Zn-doped In_2O_3 hollow spheres (the molar ratio of In/Zn is 9:1), TEM and EDX spectroscopy, along with the SAED pattern, were obtained. Fig 3(b-c) shows the TEM images before calcination, which exhibit that the spheres were

hollow, with a diameter of 200-300 nm, but the thickness of the shells is heterogeneous, the diameter of the shells even reached to 100 nm. After calcination at 500 °C for 2 h, the Zn-doped In_2O_3 hollow spheres were being perfected effectively, the diameter of the shells decreased and tend to be uniform, as shown in Fig 3(e-f). There exist a strong contrast between the light centre and the relatively dark edge provides the evidence for the hollow nature of the product, the thickness of the shells is uniform (7-40 nm), the diameter of the Zn-doped In_2O_3 hollow spheres is 200-300 nm, which is consistent with the value estimated in SEM image (Fig. 2d). Above all, the calcination never destroys the surface morphology of the Zn-doped In_2O_3 hollow spheres.

The size of the crystallites was calculated by the Scherrer formula, as shown in Table 2, and the results were 6.83, 6.90, 6.67, 6.54, 7.28, 7.72 nm for S1, S2, S3, S4, S5 and S6, respectively. Compare the value estimated from the SEM and TEM images, the Zn-doped In_2O_3 hollow spheres are consist of 1-7 of the primary particles calculated by XRD peak broadening, this feature gives evidence that the Zn-doped In_2O_3 hollow spheres are constructed by small nanoparticles, most likely through a mechanism of ''oriented attachment'' [26].

The EDX spectroscopy (Fig. 3g) shows that the Zn-doped In_2O_3 hollow spheres are elementally composed of In, Zn and O. The atomic ratio for In, Zn and O calculated from the EDX analysis was In/Zn/O = 34.32: 3.61: 61.75 (atomic ratio), which is in agreement with the value estimated from the ICP-MS. Fig. 3h shows a SAED pattern taken from the corresponding area. The SAED of the In_2O_3 structures is consistent with cubic In_2O_3 with strong ring patterns due to (222), (400), (440), and (622) planes. The results agree with XRD patterns very well.
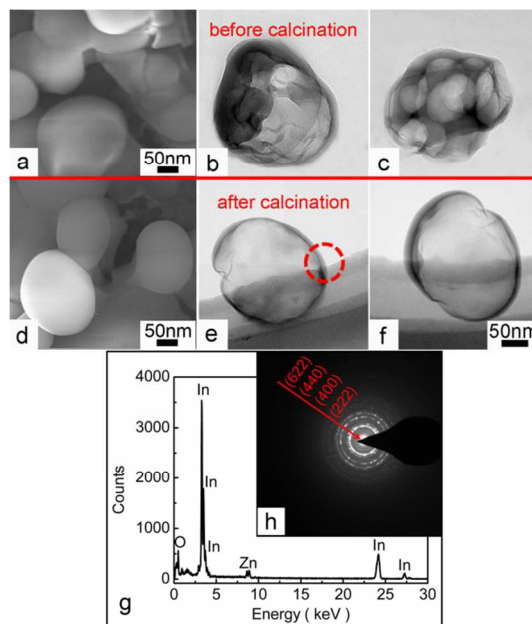
Fig. 3 SEM image (a) and TEM images (b, c) of S4 before calcination, SEM image (d) and TEM images (e, f) of S4 after calcination at 500 °C for 2 h, EDX spectroscopy (g) and SAED pattern (h) taken from the corresponding area of TEM image (e).

A two-step mechanism is proposed here for the formation of the Zn-doped In_2O_3 hollow spheres: (1) the "oriented attachment" growth step. Compared the results calculated by the Scherrer

formula to the diameters determined by microscopic techniques, the In_2O_3 hollow spheres prepared via mild chemical route are made up of smaller In_2O_3 crystals. But these small crystals have a tendency to aggregate again due to the minimization of total
[5] surface energy [27], so the lifetime is short of these small crystals. When some structure-directing agents (e.g. $NH_3 \cdot H_2O$ and formamide) are present, the gas bubbles formed in water solution provide the aggregation centres for crystal grains. Then these small crystals would aggregate around the localized regions
[10] where concentrations of NH_4^+ and formamide are relatively high, which was also driven by the minimization of interfacial energy [28]. In this stage, formamide played an important role in the formation of regular hollow spheres, based on the increased viscosity of the solution caused by formamide. The increased
[15] viscosity would reinforce and stabilize the gas bubbles, which are used to form regular hollow cores. Furthermore, the increased viscosity will slow down the movement rate of small crystals, and the slow movement rate allows small crystals to have enough time to aggregate into regular round spheres [29]. Moreover, the
[20] gas bubbles produced by NH_4^+ and formamide prevented the small crystals from aggregating into fill spheres. As the reaction proceeded continuously, more and more small crystals moved and aggregated around the surface of hollow spheres, as for larger particles, the decrease in the energy is much larger than small-
[25] sized nanoparticles. Consequently, the process in which the freshly formed small nanopartilces self-assemble to larger spherical particles is a spontaneous process [30]. (2) the hollowing step. The preformed nuclei centre (NH_4^+ and formamide) was cleared away by washing, then the $In(OH)_3$
[30] hollow spheres were obtained. After calcination the precursor of $In(OH)_3$ hollow spheres, the In_2O_3 spheres were remained hollow without deformation in the structures, as shown in TEM images. Furthermore, the hollow spheres were being perfected effectively, the diameter of the shells decreased, and the diameter size
[35] distribution tend to be uniform, thus hollow spheres with homogeneous and smooth shell were formed finally. It is well known that the larger ionic radius induces the higher diffusion barrier, so the diffusion coefficient is lower with a bigger radius [31]. Because of the larger size of indium ions (In^{3+}: 80 pm, Zn^{2+}:
[40] 74 pm), the inward diffusion of zinc ions is faster than the outward diffusion of indium ions, the gradual inward diffusion of zinc ions leads to an increase in the overall size of the particles during the conversion process. So, as the amount of Zn-added increased, the diameter of Zn-doped In_2O_3 hollow spheres
[45] enlarged, as shown in Fig. 2(b-f). More details of the formation mechanism of Zn-doped In_2O_3 hollow spheres need further investigation.

Determination of specific surface area

Fig. 4a and Supplemental Fig. I (a-e) show the N_2
[50] adsorption/desorption isotherms of the pure In_2O_3 and Zn-doped In_2O_3 structures. According to the IUPAC classification, the similar N_2 adsorption/desorption isotherms of the six samples can be classified as a type IV isotherm, with a hysteresis loop where desorption required definitively higher energy than adsorption.
[55] The isotherms of the Zn-doped In_2O_3 hollow spheres (the molar ratio of In/Zn is 9:1) show a hysteresis loop at a relatively high pressure indicating its largest surface area. The amount of N_2 adsorbed was higher for S4 (209.1 cm^3/g) than S1 (152.4 cm^3/g), S2 (162.3 cm^3/g), S3 (173.9 cm^3/g), S5 (137.6cm^3/g), or S6

[60] (116.3 cm^3/g).

The single point surface area was considerably the largest for the Zn-doped In_2O_3 hollow spheres (the molar ratio of In/Zn is 9:1) compared to the other samples, as shown in Fig. 4b. The increasing in surface area is due to its well-organized spherical
[65] feature, which is proved by the SEM and TEM images. The larger surface area, the more facilitate of the mass Cl_2 transport in the material. So the Zn-doped In_2O_3 hollow spheres (the molar ratio of In/Zn is 9:1) may possess excellent gas sensing characteristics.
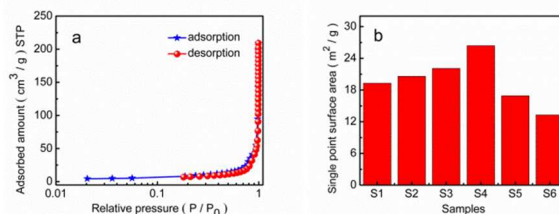
[70] Fig. 4 (a) N_2 adsorption/desorption curves of the Zn-doped In_2O_3 hollow spheres (S4), and (b) the single point surface area of S1-S6.

Gas sensing properties

Fig. 5a shows the relation between the resistance and the
[75] different amount of Zn-doped sensors exposed to 50 ppm Cl_2 at 300 °C. Upon introduction of Zn, the resistance in air decreased, while the resistance in Cl_2 atmosphere increased, and the relative resistance difference value increased. According to Fig. 5a, the sensor based on Zn-doped In_2O_3 hollow spheres (S4) has a largest
[80] relative resistance difference value, so the sensor may possess the highest response. Moreover, it can be seen from Fig. 5b that the response of each sensor increased with the increased concentration of Cl_2. The sensors based on Zn-doped In_2O_3 samples to each Cl_2 concentration exhibit higher response than
[85] those based on pure In_2O_3. The appropriate addition of Zn would be beneficial to the improvement of gas sensing properties, but superabundant addition may reduce the available adsorption sites and worsen the gas sensing properties [32]. It reveals that the sensor with In/Zn molar ratio of 9:1 has the highest response
[90] which can reach 94.7 ± 8.6, 262.2 ± 15.5, 445.7 ± 28.5, 927.6 ± 68.8, and 1296.2 ± 95.1 to 5, 10, 30, 50, and 100 ppm Cl_2, respectively. Therefore, the following study of the selectivity was focused on the sensor with In/Zn molar ratio of 9:1.
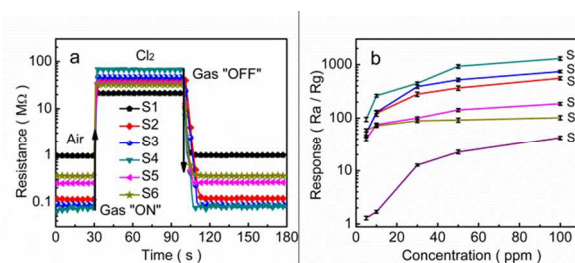
[95] Fig. 5 Gas response of sensors as a function of sample (a) typical response and recovery curve of sensors based on samples with different amount of Zn-doped exposed to 50 ppm Cl_2 at 300 °C, (b) gas response of the sensors based on samples with different amount of Zn-doped exposed to Cl_2 at concentrations ranging from 5 to 100 ppm at 300 °C. The error
[100] bars mean the standard deviation between the three times in the gas sensing testing of all the three sensors made by the same fabrication process

Considering the response of gas sensor is greatly influenced by operating temperature, parallel experiments were carried out in

the range of 80-300 °C to optimize the proper working temperature of the sensor. Fig. 6a shows the relation between the resistance and the operating temperature of Zn-doped In_2O_3 hollow spheres (the molar ratio of In/Zn is 9:1) sensor. The resistance in air decreased with increase of temperature in the range of 80-300 °C, while the resistance in Cl_2 atmosphere increased, and the relative resistance difference value increased. Moreover, it can be seen from Fig. 6b that the response of the sensor based on Zn-doped In_2O_3 hollow spheres (the molar ratio of In/Zn is 9:1) increased with the operating temperature and reached a maximum value of 927.6 ± 68.8 for 50 ppm Cl_2 at 300 °C. Therefore, the best operating temperature was determined to be 300 °C for the subsequent detections of Zn-doped In_2O_3 hollow spheres.
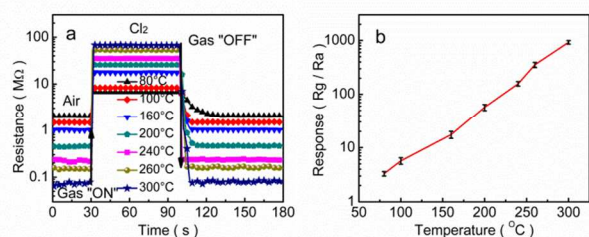
Fig. 6 Gas response of sensor as a function of sample (a) typical response and recovery curve of sensor based on Zn-doped In_2O_3 hollow spheres (the molar ratio of In/Zn is 9:1) exposed to 50 ppm Cl_2 at different working temperatures, (b) temperature dependence of the sensor gas response to 50 ppm Cl_2. The error bars mean the standard deviation between the three times in the gas sensing testing of all the three sensors made by the same fabrication process
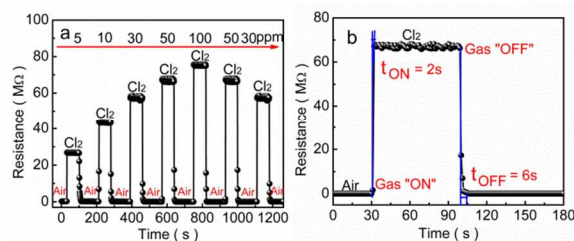
Fig. 7 Gas response of the sensor based on Zn-doped In_2O_3 hollow spheres (the molar ratio of In/Zn is 9:1) exposed to Cl_2 at (a) concentrations ranging from 5 to 100 ppm at 300 °C and (b) 50 ppm

Fig. 7a illustrates the typical response recovery characteristics of the sensor based on Zn-doped In_2O_3 hollow spheres (the molar ratio of In/Zn is 9:1) to Cl_2 with concentrations of 5, 10, 30, 50, and 100 ppm at 300 °C. The sensor exhibited excellent response when exposed to various Cl_2 concentrations. When exposed to 5 ppm Cl_2, the response was 94.7 ± 8.6, indicating that high gas response can be achieved in detecting low concentration Cl_2 by using Zn-doped In_2O_3 hollow spheres as sensing material. With an increase of the Cl_2 concentration, the response increased dramatically. Furthermore, the sensor showed a quick response and short recovery time. When exposed to 50 ppm Cl_2, the response and recovery time (defined as the time required reaching 90 % of the final equilibrium value) is 2 s and 6 s, respectively, as shown in Fig. 7b.

To investigate the Cl_2 selectivity of the sensor, the Zn-doped In_2O_3 hollow spheres (the molar ratio of In/Zn is 9:1) sensor was tested at 50 ppm Cl_2 and the same concentration of other gases, including toluene, acetone, ammonia, NO_2, H_2S, formaldehyde and gasoline. The results are shown in Fig. 8. As can be seen, the gas response to Cl_2 is significantly higher than that to the other tested gases, with a magnitude about 16-618 times greater to 50 ppm Cl_2 than that for all the other tested gases under the same concentration. According to the experimental results, the Zn-doped In_2O_3 hollow spheres sensor can selectively detect Cl_2 with the interference of other gases.
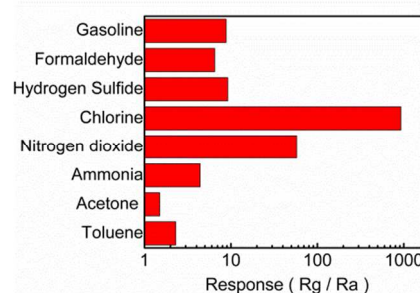
Fig. 8 Selectivity of the Zn-doped In_2O_3 hollow spheres (the molar ratio of In/Zn is 9:1) sensor to different test gases with a concentration of 50 ppm at 300 °C
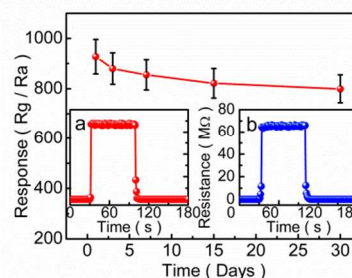
Fig. 9 Stability of Zn-doped In_2O_3 hollow spheres (the molar ratio of In/Zn is 9:1) sensor to Cl_2 with a concentration of 50 ppm at 300 °C. (inset: (a) gas response of the sensor for the first day (b) the 30th). The error bars mean the standard deviation between the three times in the gas sensing testing of all the three sensors made by the same fabrication process

Fig. 9 displays the stability of the sensor based on Zn-doped In_2O_3 hollow spheres (the molar ratio of In/Zn is 9:1) to Cl_2 with a concentration of 50 ppm at 300 °C. The results shows that the response decreases overtime, but the response was still very high even after 30 days. So the Zn-doped In_2O_3 hollow spheres (the molar ratio of In/Zn is 9:1) sensor is an excellent gas sensor material.

Gas sensing mechanism

Based on the above results, the Zn-doped In_2O_3 hollow spheres sensor shows an improved sensing property compared with pure In_2O_3 sensor. The gas sensing mechanism of Cl_2 has been widely invested so far [33-35]. Herein, we only exposed the higher sensing properties of the sensor based on Zn-doped In_2O_3 structures, which in contrast to the non-doped structures.

From the SEM images, the doping of Zn significantly affects the overall morphology, and affects the specific surface area of In_2O_3. The enhanced sensing performance of the Zn-doped In_2O_3

hollow spheres can be ascribed to its large BET surface area. As the Zn-doped In_2O_3 hollow spheres (the molar ratio of In/Zn is 9:1) had the largest BET surface area (26.4 m^2/g), the sensor could absorb more Cl_2, the resistance's increasing and the resistance's decreasing became more notable, which can enhance its sensing performance. The large BET surface area increased the accessible surface area and facilitated the mass transport of gas in the material, which is in favour of their applications in fields such as catalysis and sensing. With further increasing of Zn, the diameter of spheres increased and aggregated to form some irregular spheres and cubes, the larger diameter and irregular shape destroy the morphology and decrease the BET surface area of In_2O_3, which may affect the Cl_2 sensing performance.

In_2O_3 is n-type semiconductive oxides which conduction electrons come primarily from point defects (oxygen vacancies and interstitial metal atoms). For metal oxide gas sensors, the change of resistance is mainly caused by the adsorption and desorption of gas molecules on the surface of the sensing structure. First, oxygen species were adsorbed on the surface of particles in the air, and then were ionized into O^-_{ads} or O^{2-}_{ads} by capturing free electrons from the particles, thus leading to the formation of thick space charge layer and increasing of surface band bending. Nandan Singh et al. [36] have found that the Zn-doping can increase the oxygen vacancies and surface defects significantly, while the oxygen vacancies and surface defects can play a role of as the preferential adsorption for a gas molecule [37]. Due to the chemical potential gradient between semiconducting Zn-doped In_2O_3 hollow spheres and Cl_2, electrons transfer from Zn-doped In_2O_3 to Cl_2 molecule. Cl_2 acts as an electron acceptor in the reaction, resulting in the increase of the resistance of the sensor. On the other hand, the trapped electrons are released to the Zn-doped In_2O_3 hollow spheres by Cl_2 after stopping the supply of Cl_2, leading to a decrease of the resistance. When Cl_2 molecules adsorb onto the Zn-doped In_2O_3 hollow spheres surface, electrons transfer from a higher chemical potential to the material with a lower chemical potential until the system reaches equilibrium. For the Zn-doped In_2O_3 hollow spheres, there is a larger chemical potential gradient between the adsorbed Cl_2 molecules compared to the undoped In_2O_3. This results in the more electron transfer (to reach equilibrium) and therefore increase the gas sensing performance of the Zn-doped In_2O_3 hollow spheres.

The sensor electrical resistances of pure In_2O_3 and Zn-doped In_2O_3 hollow spheres (the molar ratio of In/Zn is 9:1) in 50 ppm Cl_2 at 300 °C were 21.3 and 67.1 MΩ, respectively. While the sensor electrical resistances in air were 958.7 and 73.1 kΩ, respectively. Therefore, the chemical absorbed oxygen (O_2^-) in In_2O_3 and Zn lattice and the releasing electrons from the accumulation layer together, making the output voltage of Zn-doped In_2O_3 hollow spheres sensor decreased sharply when contact with Cl_2 [38-39]. More details of the enhancing effect of the Zn-doped In_2O_3 hollow spheres on sensing properties need further investigation.

Conclusions

In summary, Zn-doped In_2O_3 hollow spheres were synthesized by a facile solution reaction without any surfactant and template. SEM images showed the molar ratios of In/Zn effect profoundly on particle size and morphologies of Zn/In_2O_3 composites and the Zn-doped In_2O_3 hollow spheres was obtained when the molar ratio of In/Zn is 9:1. A possible growth mechanism of Zn-doped In_2O_3 hollow spheres has also been proposed. The gas sensing measurements demonstrated that the Zn-doped In_2O_3 hollow spheres (the molar ratio of In/Zn is 9:1) sensor had the highest response. This is possibly due to the large specific surface area of the Zn-doped In_2O_3 hollow spheres. Therefore, it is expected that this facile route prepared the Zn-doped In_2O_3 hollow spheres would be an ideal candidate for applications in Cl_2 sensors.

Notes and references

[a] state Key Laboratory of Solidification Processing, School of Materials Science and Engineering, Northwestern Polytechnical, Xi'an, China. Tel: +86-29-88494463; E-mail: hqfan3@163.com;lipei8143706@163.com;

Reference:
[1] V. D. Kapsea, S. A. Ghosha, G. N. Chaudharib, F. C. Raghuwanshic, Nanocrystalline In_2O_3-based H_2S sensors operable at low temperatures, Talanta 76 (2008) 610-616.
[2] N. Guillet, R. Lalauze, J. P. Viricelle, C. Pijolat, L. Montanaro, Development of a gas sensor by thick film technology for automotive applications: choice of materials-realization of a prototype, Mater. Sci. Eng. C 21 (2002) 97-103.
[3] P. S. More, Y. B. Khollam, S. B. Deshpande, S. K. Date, N. D. Sali, S. V. Bhoraskar, S. R. Sainkar, R. N. Karekar, R. C. Aiyer, Introduction of delta-Al_2O_3/Cu_2O material for H_2 gas-sensing applications, Mater. Lett. 58 (2004) 1020-1025.
[4] L. Wang, R. V. Kumar, Thick film miniaturized HCl gas sensor, Sens. Actuators B 98 (2004) 196-203.
[5] L. Y. Chen, Z. D. Zhang, Biomolecule-assisted synthesis of $In(OH)_3$ hollow spherical nanostructures constructed with well-aligned nanocubes and their conversion into C-In_2O_3, J. Phys. Chem. C 112 (2008) 18798-18803.
[6] V. Romanovskaya, M. Ivanovskaya, P. Bogdanov, A study of sensing properties of Pt- and Au-loaded In_2O_3 ceramics, Sens. Actuators B 56 (1999) 31-36.
[7] A. Qurashi, E. M. El-Maghraby, T. Yamazaki, T. Kikuta. Catalyst supported growth of In_2O_3 nanostructures and their hydrogen gas sensing properties, Sens. Actuators B 147 (2010) 48-54.
[8] N. Singh, C. Y. Yan, P. S. Lee, Room temperature CO gas sensing using Zn-doped In_2O_3 single nanowire field effect transistors, Sens. Actuators B 150 (2010) 19-24.
[9] H. Yamaura, Y. Iwasaki, S. Hirao, H. Yahiro, CuO/SnO_2-In_2O_3 sensor for monitoring CO concentration in a reducing atmosphere, Sens. Actuators B 153 (2011) 465-467.
[10] X. J. Xu, H. T. Fan, Y. T. Liu, L. J. Wang, T. Zhang, Au-loaded In_2O_3 nanofibers-based ethanol micro gas sensor with low power consumption, Sens. Actuators B 160 (2011) 713-719.
[11] S. J. Kim, I. S. Hwang, J. K. Choi, Y. C. Kang, J. H. Lee, Enhanced C_2H_5OH sensing characteristics of nano-porous In_2O_3 hollow spheres prepared by sucrose- mediated hydrothermal reaction, Sens. Actuators B 155 (2011) 512-518.
[12] M. Epifani, E. Comini, J. Arbiol, R. Díaz, N. Sergent, T. Pagnier, P. Siciliano, G. Faglia, J. R. Morante, Chemical synthesis of In_2O_3

nanocrystals and their application in highly performing ozone-sensing devices, Sens. Actuators B 130 (2008) 483-487.

[13] J. B. Mu, B. Chen, M. Y. Zhang, Z. C. Guo, P. Zhang, Z. Y. Zhang, Y. Y. Sun, C. L. Shao, Y. C Liu, Enhancement of the visible-light photocatalytic activity of In_2O_3-TiO_2 nanofiber heteroarchitectures, Appl. Mater. Interfaces 4 (2012) 424-430.

[14] T. J. Yan, X. X. Wang, J. L. Long, P. Liu, X. L. Fu, G. Y. Zhang, X. Z. Fu, Urea-based hydrothermal growth, optical and photocatalytic properties of single-crystalline $In(OH)_3$ nanocubes, J. Colloid Interface Sci. 325 (2008) 425-431.

[15] L. Xu, H. W. Song, B. Dong, Y. Wang, J. S. Chen, X. Bai, Preparation and bifunctional gas sensing properties of porous In_2O_3-CeO_2 binary oxide nanotubes, Inorg. Chem. 49 (2010) 10590-10597.

[16] P. Li, Y. Cai, H. Q. Fan, Porous thin sheet-based α-Fe_2O_3-doped In_2O_3 structures: hydrothermal synthesis and enhanced Cl_2 sensing performance, RSC Adv. 3 (2013) 22239-22245.

[17] E. Li, Z. X. Cheng, J. Q. Xu, Q. Y. Pan, W. J. Yu, Y. L. Chu, Indium oxide with novel morphology: synthesis and application in C_2H_5OH gas sensing, Cryst. Growth Des. 9 (2009) 2146-2151.

[18] W. Y. Yin, J. Su, M. H. Cao, C. Y. Ni, C. W. Hu, B. Q. Wei, In_2O_3 nanorod bundles derived from a novel precursor and In_2O_3 nanoaggregates: controllable synthesis, characterization, and property studies, J. Phys. Chem. C 114 (2010) 65-73.

[19] J. Y. Liu, T. Luo, F. L. Meng, K. Qian, Y. T. Wan, J. H. Liu, Porous hierarchical In_2O_3 micro-/nanostructures: preparation, formation mechanism, and their application in gas sensors for noxious volatile organic compound detection, J. Phys. Chem. C 114 (2010) 4887-4894.

[20] A. Datta, S. K. Panda, D. Ganguli, P. Mishra, S. Chaudhuri, In_2S_3 micropompons and their conversion to In_2O_3 nanobipyramids: simple synthesis approaches and characterization, Cryst. Growth Des. 7 (2007) 163-169.

[21] S. T. Jean, Y. C. He, Growth mechanism and photoluminescence properties of In_2O_3 nanotowers, Cryst. Growth Des. 10 (2010) 2014-2110.

[22] H. Huang, E. E. Remsen, T. Kowalewski, K. L Wooley, Nanocages derived from shell cross-linked micelle templates, J. Am. Chem. Soc. 121 (1999) 3805-3806.

[23] C. E. Fowler, D. Khushalani, S. Mann, Interfacial synthesis of hollow microspheres of mesostructured silica, Chem. Commun. 19 (2001) 2028-2029.

[24] B. X. Li, Y. Xie, M. Jing, G. X. Rong, Y. C. Tang, G. Z. Zhang, In_2O_3 hollow microspheres: synthesis from designed $In(OH)_3$ precursors and applications in gas sensors and photocalysis, Langmuir 22 (2006) 9380-9385.

[25] P. Li, H.Q. Fan, Y. Cai, In_2O_3/SnO_2 heterojunction microstructures: Facile room temperature solid-state synthesis and enhanced Cl_2 sensing performance, Sens. Actuators B 185 (2013) 110-116.

[26] M. L. Zhao, G. S. Li, J. Zheng, L. P. Li L. S. Yang, Fabrication of assembled-spheres YVO_4:(Ln^{3+}, Bi^{3+}) towards optically tunable emission, CrystEngComm 14 (2012) 2062-2070.

[27] L. Gou, F. Liang, X. G. Wen, S. H. Yang, L. He, W. Z. Zheng, C. P. Chen, Q. P. Zhong, Uniform magnetic chains of hollow cobalt mesospheres from one-pot synthesis and their assembly in solution, Adv. Funct. Mater. 17 (2007) 425-430.

[28] X. Liu, Y. F. Li, W. W. Zhu, P. F. Fu, Building on size-controllable hollow nanospheres with superparamagnetism derived from solid Fe_3O_4 nanospheres: preparation, characterization and application for lipase immobilization, CrystEngComm 15 (2013) 4937-4947.

[29] G. Z. Wang, R. Saeterli, P. M. Rorvik, A. T. J. Helvoort, R. Holmestad, T. Grande, M. A. Einarsrud, Self-assembled growth of $PbTiO_3$ nanoparticles into microspheres and bur-like structures, Chem. Mater. 19 (2007) 2213-2221.

[30] X. L. Cheng, J. S. Jiang, M. Hu, G. Y. Mao, Z. W. Liu, Y. Zeng, Q. H. Zhang, Liquid-liquid interface-assisted solvothermal synthesis of durian-like α-Fe_2O_3 hollow spheres constructed by nano-polyhedrons, CrystEngComm. 14 (2012) 3056-3062.

[31] A. M. Asaduzzaman, F. Y. Wang, G. Schreckenbach, Quantum-chemical study of the difffusion of Hg(0, I, II) into the ice(Ih), J. Phys. Chem. C 116 (2012) 5151-5154.

[32] L. M. Huang, H. Q. Fan, Room-temperature solid state synthesis of ZnO/α-Fe_2O_3 hierarchical nanostructures and their enhanced gas-sensing properties, Sens. Actuators B 171-172 (2012) 1257-1263.

[33] J. Tamaki, J. Niimi, S. Ogura, S. Konishi, Effect of micro-gap electrode on sensing properties to dilute chlorine gas of indium oxide thin film microsensors, Sens. Actuators B 117 (2006) 353-358.

[34] D. R. Patil, L. A. Patil, Room temperature chlorine gas sensing using surface modified ZnO thick film resistors, Sens. Actuators B 123 (2007) 546-553.

[35] W. Ding, P. Hu, J. Q. Xu, X. W. Dong, Y. Z. Pan, Fast response chlorine gas sensor based on mesoporous SnO_2, Sens. Actuators B 140 (2009) 383-389.

[36] N. Singh, C. Y. Yan, P. S. Lee, Room temperature CO gas sensing using Zn-doped In_2O_3 single nanowire field effect transistors, Sens. Actuators B 150 (2010) 19-24.

[37] M. W. Ahn, K. S. Park, J. H. Heo, J. G. Park, D. W. Kim, K. J. Choi, J. H. Lee, S. H. Hong, Gas sensing properties of defect controlled ZnO-nanowire gas sensor, Appl. Phys. Lett. 93 (2008) 263103/1-263103/3.

[38] Z. Ling, C. Leach, R. Freer, NO_2 sensitivity of a heterojunction sensor based on WO_3 and doped SnO_2, J. Eur. Ceram. Soc. 23 (2003) 1881-1891.

[39] A. Chen, X. Huang, Z. Tong, S. Bai, R. Luo, C. Liu, Preparation, characterization and gas-sensing properties of SnO_2-In_2O_3 nanocomposite oxides, Sens. Actuators B 115 (2006) 316-321.